

Article

Coating Deterioration and Underlying Metal Corrosion Processes in Water-Line Area: Role of DACs

Zhiwei Chen ^{1,2} , Wei Zhang ^{1,2,*}, Yi Zhan ^{1,2}, Bing Lei ^{1,2}, Tianying Sun ^{1,2} and Weihua Li ^{1,2,3,*}

¹ School of Chemical Engineering and Technology, Sun Yat-sen University, Zhuhai 519082, China; chenzhw58@mail2.sysu.edu.cn (Z.C.); zhany9@mail.sysu.edu.cn (Y.Z.); leibing@mail.sysu.edu.cn (B.L.); sunt23@mail.sysu.edu.cn (T.S.)

² Southern Marine Science and Engineering Guangdong Laboratory (Zhuhai), Zhuhai 519082, China

³ Key Laboratory of Marine Environmental Corrosion and Bio-fouling, Institute of Oceanology, Chinese Academy of Sciences, Qingdao 266071, China

* Correspondence: zhangw286@mail.sysu.edu.cn (W.Z.); liweihua3@mail.sysu.edu.cn (W.L.)

Received: 1 July 2020; Accepted: 13 July 2020; Published: 16 July 2020



Abstract: Water-line corrosion is a highly concentrated type of localized corrosion. The conventional single electrode method is limited in its ability to obtain the kinetic information of the corrosion occurrence and development processes. Herein, the coating deterioration and underlying metal corrosion processes in water-line area were studied by a small wire beam electrode to monitor the current density distribution. The distance between each electrode was very small (interval: 0.3 mm), thus facilitating it to approach the practical metal component with a continuous surface. The results showed that cathodic and anodic sites tended to be weak points of the coating at the initial stage. With the continuous degradation of the coating, the cathodic zone tended to occur in the above the anodic zone due to the effect of differential aeration cells (DACs). Subsequently, the cathodic zone expanded to the waterline and the polarity reversed to the anodic zone, causing the coating to peel and blister continuously from the bottom up. When the cathodic zone extended to the gas phase area above the water line, this area became the strongest cathodic zone under the action of the thin liquid film, thus significantly accelerating the corrosion of the base metal at the bottom. The present study aims to achieve an in-depth understanding of coating deterioration and underlying metal corrosion processes in the water-line area, providing a new means of directly visualizing the role of DACs played in water line corrosion.

Keywords: water-line corrosion; wire beam electrode; coating deterioration; metal corrosion

1. Introduction

The phenomenon of water-line corrosion (WLC) that occurs along the gas–liquid–solid three-phase interface is generally considered to result from differential aeration cells (DACs) adjacent to the water line [1]. The area above the water level is highly oxygenated and acts as a cathode, while the part below is less oxygenated and behaves as an anode [2]. Coating deterioration and underlying metal corrosion adjacent to the water line is an intractable problem. To the best of our knowledge, extensive research work has not been carried out in this area thus far.

Many strategies have been employed to study the WLC phenomenon. Jeffrey and Melchers used a raft to study the steel corrosion loss profiles adjacent to the water line in calm, natural seawater. In all cases, mass loss rapidly increased to peak at about 250 mm above the water line. The high corrosion loss observed around 200 mm below the water line in the experiment was consistent with the results of classical laboratory studies [3]. This indicated that it was the result of DACs with the well-aerated

immediate water-line region becoming cathodic to the less well-aerated immersed parts of the steel strip that became anodic. Based on the topography of the corroded surfaces below the water line, the authors speculated that there might be the formation of one or more cathodic regions further down in the immersed zone.

However, due to the lack of in-situ electrochemical information, it is obviously difficult to obtain accurate information about alternating cathodic–anodic processes and corrosion dynamics via the microscopic observations and weight-loss measurement [4]. The wire beam electrode (WBE) method is an in-situ electrochemical technique capable of measuring surface potential and current distribution, especially for complex multi-interface corrosive systems.

Tan used WBE to study the long-term corrosion behavior of carbon steel in the water-line area [5]. The calculated corrosion results based on the instantaneous corrosion rate were found to be consistent with the microscopically observed corrosion depth. The WLC development processes of carbon steel in static 3.5 wt.% NaCl solution were studied by the WBE technique [6]. In the initial stage, the cathodic and anodic sites were cross-distributed. Subsequently, under the influence of the DACs, the cathodic region moved toward the vicinity of the water line, and the anodic region appeared at the lower portion of it. Notably, the cathodic region moved continuously to the upper part of the water line, crossing the gas/liquid interface into the atmospheric zone. Therefore, when the current and distribution of cathodic and anodic regions reached a stable level, the main cathode region was located above the water line and the corrosion rate became stable.

In the water-line area, the coating undergoes accelerated deterioration and the base metal undergoes localized non-uniform corrosion. However, there are many issues in the process of coating degradation and metal corrosion under waterline that need to be studied; for example, which stages of coating degradation and metal corrosion are affected by water permeation and DACs, respectively, and the extent of influence on each stage. To resolve these issues, we studied the coating deterioration and underlying metal corrosion process in the water-line area by a small WBE. In addition, studying the mechanism of coating degradation and metal corrosion in water-line area can be of great value for the development of WLC-resistance coating and optimization of evaluation methods.

2. Experimental

Figure 1 displays a schematic diagram of the experimental setup required for the water-line experiment. The WBE was fabricated by arranging carbon steel (material: Q235, diameter: 1.2 mm, interval: 0.3 mm) into a 11×11 matrix, sealed by epoxy (Figure 1a). The working surfaces of WBE were abraded with silicon carbide papers up to 1000# and rinsed with distilled water and ethanol before being dried using a hairdryer. As a demonstration, the red iron oxide phenolic resin primer was utilized as the coating and applied on the working surface and then placed in a dust shield for 7 days. The thickness of the coating was $80 \pm 5 \mu\text{m}$. NaCl solution (3.5 wt.%) was used as the electrolyte solution.

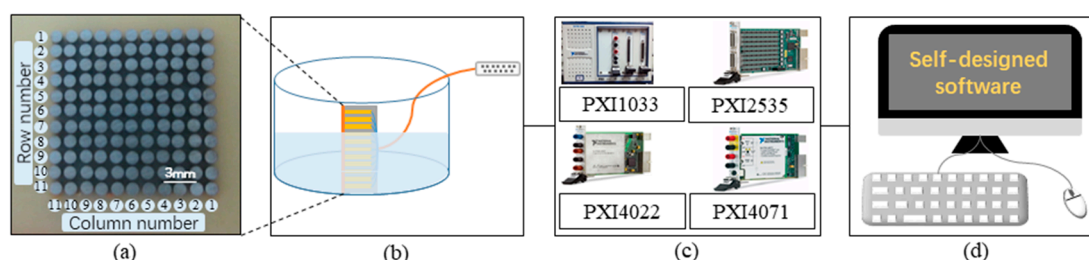


Figure 1. Schematic diagram of the experimental setup. (a) Photo of the wire beam electrode (WBE) before applying the coating on the surface. (b) Experimental device. (c) Measurement system. (d) Computer console.

The WBE was partially immersed in 3.5 wt.% NaCl solution with a volume of around 20 L under static conditions at 25 °C (Figure 1b). The position of the water line was maintained at the middle of the cylinders at the 4th row so that 3 rows were completely exposed to air and 7 rows were in the solution. Distilled water was added daily to make up for the water lost due to water evaporation.

The instrument for WBE test consists of modular instruments (National Instruments Co. NI), as shown in Figure 1c. Before the test, all electrodes in the WBE were connected to allow the electrons to flow freely. When the current distribution test started, the first electrode disconnected from the others, and the current between the individual electrode and other connected electrodes was measured. Subsequently, the first electrode re-connected to the other electrodes and the second electrode disconnected and repeated the above procedures. The abovementioned experimental process was controlled by self-designed software [7,8], as shown in Figure 1d.

3. Results and Discussion

3.1. Galvanic Current Distribution Maps of the WBE

Figure 2 displays the galvanic current distribution maps of the WBE in 3.5 wt.% NaCl for various days. In the first two days, no local high anodic or cathodic current appeared in the current distribution map, suggesting that the base metal was effectively protected by the coating and the underlying corrosion reaction did not occur. This period corresponds to the water penetration stage [9].

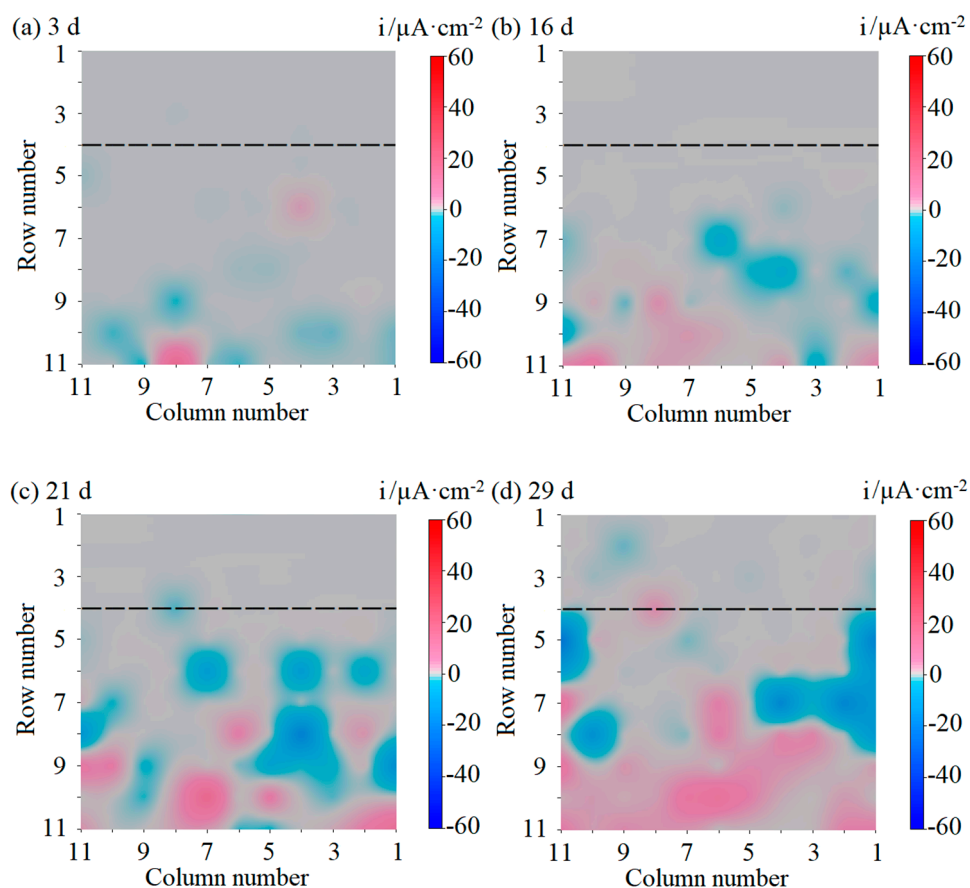


Figure 2. Cont.

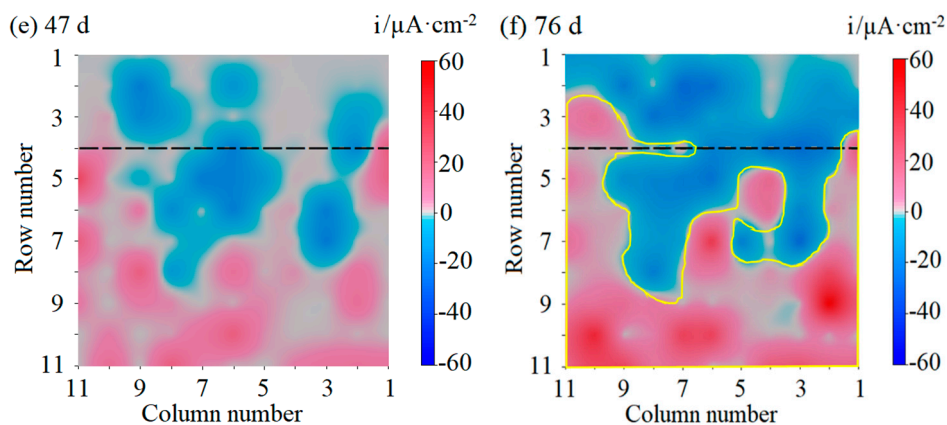


Figure 2. Galvanic current recorded on the WBE in 3.5 wt.% NaCl solution for various immersion days. (a–f) correspond to 3, 16, 21, 29, 47, and 76 days, respectively.

On the 3rd day, the anodic current was observed at the 11th row and the 8th column electrode (11–8# for short hereinafter) and 6–4# showed as anodic current on Day 3, while the cathodic current was found at 9–8#, 10–3#, and 11–10# (Figure 2a). The presence of cathodic and anodic sites indicated that water and aggressive ions had diffused to the substrate/polymer interface, thus establishing the galvanic cell and also initiating the electrochemical reaction [10]. This scattered distribution of cathodic and anodic sites is considered to be due to the non-uniform water penetration processes of the coating [11]. Hydrophilic pathways developed during water sorption from the electrolyte solution into organic coating eventually widened to form ionic transport channels connecting the substrate and electrolyte, enabling localized underfilm corrosion [12]. The distribution of these ionic transport channels on the coating surface was not uniform, causing the random distribution of cathode and anode sites.

Notably, the polarity of 9–8#, 11–1#, and 11–10#, which were located in the bottom of the electrode, reversed from cathode to anode on Day 16. In the meantime, new cathodic sites (7–11#, 8–2#, and 11–3#) appeared in the upper part of the anodic region, as shown in Figure 2b. The delamination of coating was affected by many factors, and there is no definite conclusion on the exact factors of coating delamination. The exact mechanism of coating delamination needs to be further studied. Previous studies speculated that cathodic reactions can significantly reduce the bonding force of the substrate/polymer interface and accelerate the delamination of the coating [13,14]. When vast aggressive ions penetrated into the interface, the exposed “fresh” substrate tended to be anodically dissolved.

On Day 21, the anodic sites of 7–11#, 8–2#, and 11–3# reversed to the cathodes (Figure 2c). Cathode sites such as 4–8#, 6–2#, 7–10#, 8–4#, 9–3#, 10–3#, and 11–6# were observed simultaneously. Affected by the DACs, the cathodic regions continued to expand upwards, and the uppermost area of the region reached water-line position 4–8#. Further, the anodic regions expanded upward due to the reversal of the polarity of the cathodic regions.

As the polarity of the cathodic points at the bottom of the electrode reversed to the anode on Day 29 (Figure 2d), the anodic current region was distributed in a sheet shape on the lower portion of rows 9 to 11. It should be noted that the polarity of the 4–8# at the water line reversed to the anode, and a new cathodic site (2–9#) was found in the atmospheric region above the water-line.

The cathodic sites above the water line rapidly increased on Day 47 (Figure 2e) as compared with the changes on Day 29. By the 76th day, a higher cathodic current was detected in all cylinders from the 1st to 3rd rows located above the water-line, except for two anodic sites of 3–11# and 3–10# (Figure 2f).

Statistical analysis was performed on all anodic sites (except the initial anodic sites) throughout the experimental period. These sites experienced a period of cathodic current at first and then the anodic current. Figure 3 demonstrates four electrode sites (8–4#, 11–3#, 8–11#, and 7–6#) as examples. It was concluded that the cathodic reduction reaction of dissolved oxygen in the interface region led to

the delamination of the coating from the metal surface and then induced the anodic dissolution of the base metal.

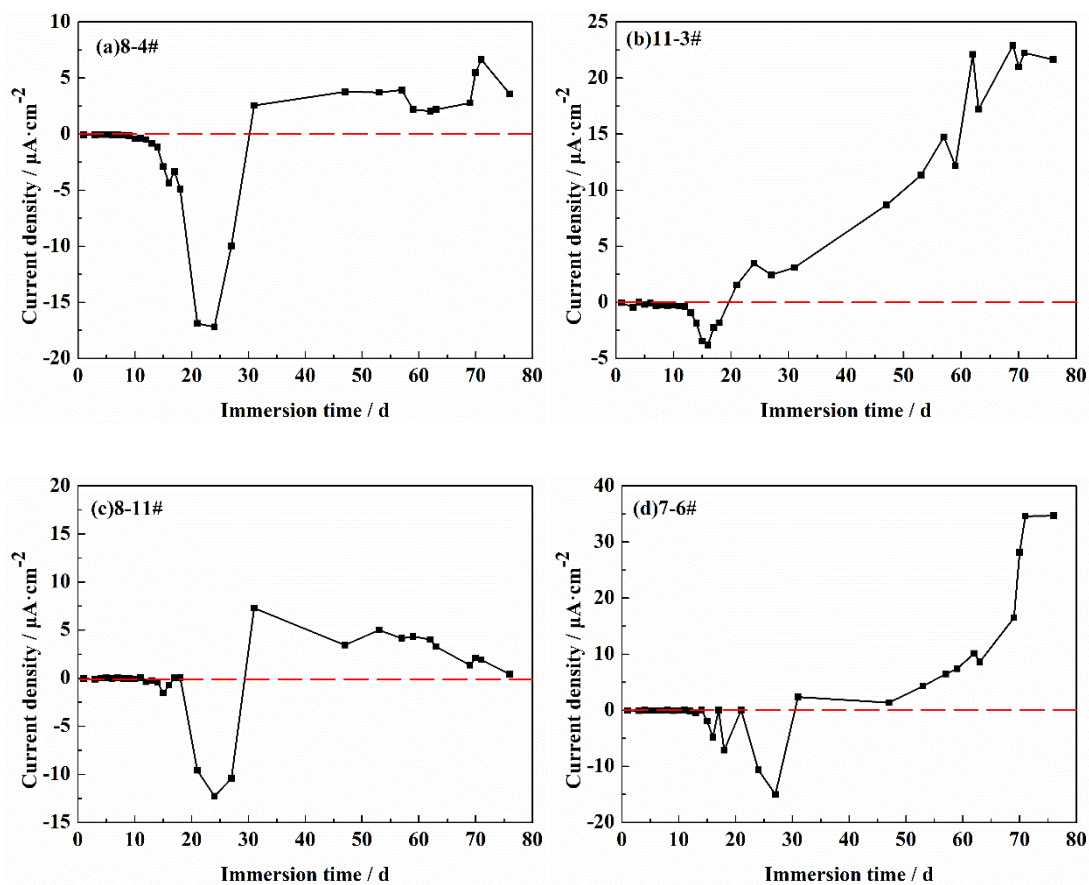


Figure 3. Current density of single electrode (a) 8–4#, (b) 11–3#, (c) 8–11# and (d) 7–6# as a function of different immersion time.

The polarity reversal of the current had been reported under the rust layer and the coating [11]. Iron in the weak points of the coating acted as the local anode, wherein iron dissolution became prominent. The delaminated part was considered as the local cathode, and within this area, only oxygen reduction took place [13]. However, the rust was also found to act as a cathodic reactant and further led to the development of new anodes beneath the coating once the rust deposited at the defects or later beneath the coating [15].

In general, the corrosive galvanic cell circuit could not form between the atmospheric and the immersion region due to the lack of electrolyte solution. Cathode and anode points with high current densities appeared in the gas phase region above the water line (Rows 1 to 3), indicating that there was an ion channel between the area and the bulk solution, forming a galvanic cell surrounding the water line. We proposed that the ion channel should be a thin liquid film on the electrode surface in the atmospheric region.

We speculate that this thin liquid film above the waterline is a “water-absorbing paint film” formed by the capillary action of the cross-linked micropores inside the organic coating. It could also be the result of the Three-Phase Boundary (TPB) spreading upward and the width increasing [16].

3.2. The Current Density Vector Sum

The degradation process of the coating is random under the influence of water penetration. In order to eliminate the impact of this random factor and better understand the effect of DACs, we introduced

the concept of single-row current density [6]. The current density of each row (11 cylinders) was added to obtain the single-row current density. Figure 4 displays the current density vector sum at various immersion times. It should be noted that if the current density of a row is positive, this does not imply that all the electrodes in the row have an anodic dissolution reaction; the reverse is the same.

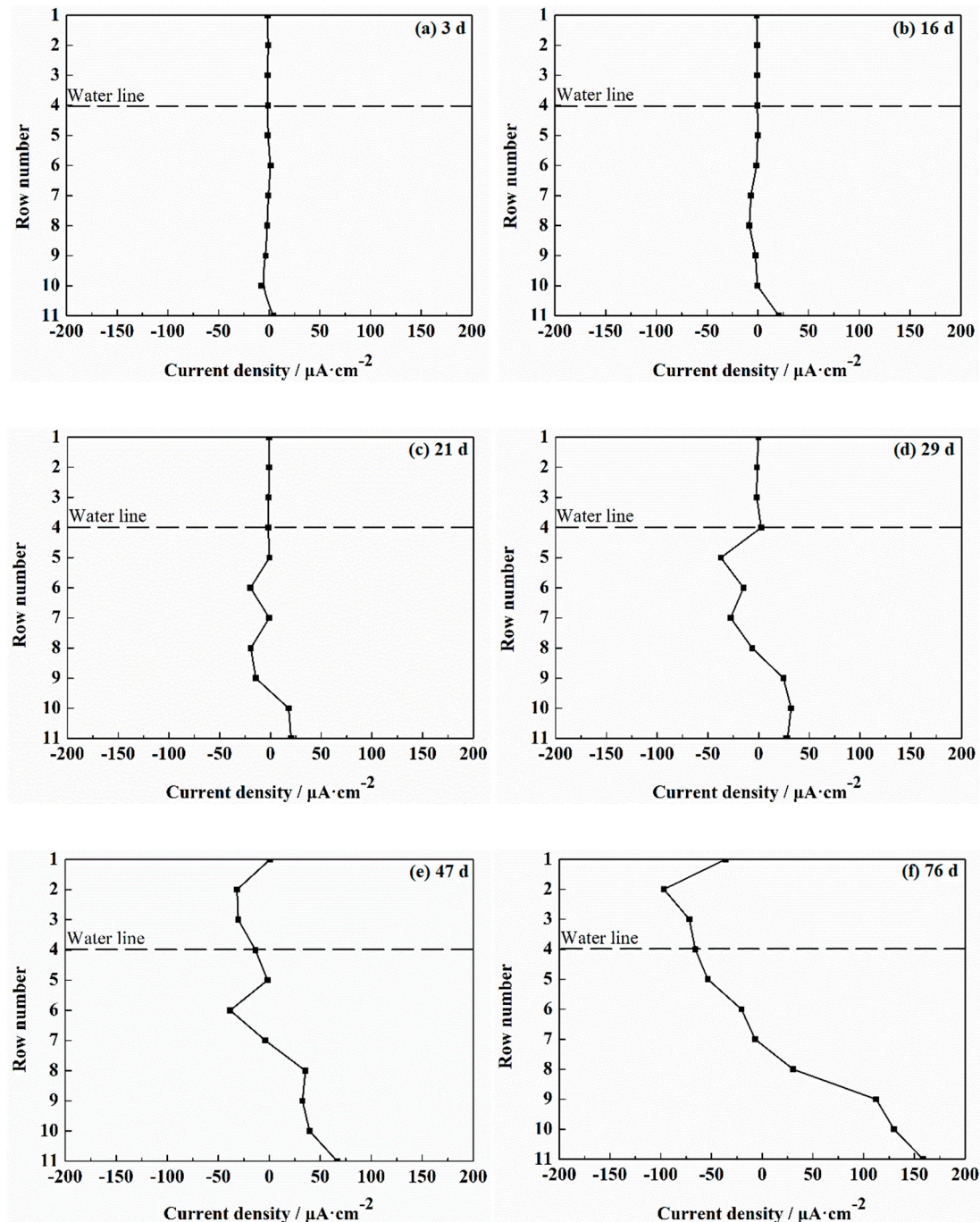


Figure 4. Single row current density vector sum at various immersion times. (a–f) correspond to 3, 16, 21, 29, 47, and 76 days, respectively.

As shown in Figure 4, the cathodic region was initially at the upper portion, while the anodic region was at the lower portion, but both the cathodic and anodic regions gradually expanded toward the water line together. For example, on Day 3, both the cathode and the anode were located in the bottom of the electrode with the 10th row acting as the cathode and the 11th row acting as the anode

(Figure 4a). On Day 16, the cathodic area extended upward to the 7th–10th rows, while the anodic area remained at the 11th row (Figure 4b). By Day 21, the cathodic region extended upward to the 6th–9th rows. The polarity of the 10th row reversed to the anode; therefore, the anode region extended upward to the 10th and 11th rows. Thereafter, the cathode region continued to expand toward the water line. As the polarity of the cathode bottom reversed, the anode region also gradually expanded upward (Figure 4c). On Day 29, the cathodic area extended to 5th–8th rows with the polarity reversal in the 9th row. The anodic area was located in the 9th–11th rows (Figure 4d). The cathodic area expanded to the 2nd–7th rows and began to enter the atmospheric area situated above the water line on Day 47. The polarity of the 8th row reversed to an anode (Figure 4e). On Day 76, the cathodic area expanded to the 1st–7th rows, and the anodic area was located in the 8th–11th rows (Figure 4f).

As the cathodic and anodic regions expanded upward, the maximum single-row cathodic and anodic currents increased gradually. When the cathodic sites entered the thin liquid film area on the water line, the vector sums of single-row current density of both the cathode and anode showed rapid increases. For instance, the current density of the 11th row was only $4.3 \mu\text{A}\cdot\text{cm}^{-2}$ on Day 3, but it rapidly increased to $20.6 \mu\text{A}\cdot\text{cm}^{-2}$ on Day 16. On Day 29, the anode current density in Row 11 was only $28.4 \mu\text{A}\cdot\text{cm}^{-2}$ when a cathodic current point was found above the water line. By 47 days, the anode current density had increased rapidly to $66.7 \mu\text{A}\cdot\text{cm}^{-2}$ as the cathode point spread above the water line. The anode current density reached $158.6 \mu\text{A}\cdot\text{cm}^{-2}$ on Day 76 when water line was almost completely occupied by the cathode.

Previous results revealed that the thin liquid film zone is a high-speed cathodic reaction region [17,18], in which the diffusion rate of oxygen is much higher than that in bulk solution [19]. Probably, this explains the largest cathode current density reaction zone spotted from Rows 1 to 3 above the water line on Day 76.

The cathodic reaction does not directly involve the loss of the metal substrate. The cathodic reaction is particularly important for two reasons. Firstly, the cathodic reaction was coupled to the anodic reaction. Impeding the cathodic reaction would also impede the anodic reaction. Similarly, accelerating the cathodic reaction would also accelerate the anodic reaction [20]. Secondly, the cathodic reaction at the coating/metal interface is an important influencing factor that destroys the adhesion between the coating and metal. On Day 76, strong cathodic reaction zones were formed in the 1st–3rd rows. Therefore, the maximum single-row anodic current density in row 11 showed a rapid increase.

3.3. Morphology of the Coating and Substrate Metal Surface

Figure 5 shows the changes in the morphology of the coating and substrate metal surface at various immersion times. The increase in corrosion current was consistent with the increase in the delamination area (also the delamination area) on the coating surface (Figures 2a–f and 5a–e). The blisters on the coating surface began to spread from the bottom of the electrode to the upward region with the progress of the cathode reaction on the electrode surface. As the delamination area continued to increase, the area of the exposed base metal increased accordingly, resulting in the gradual increase of the corrosion current.

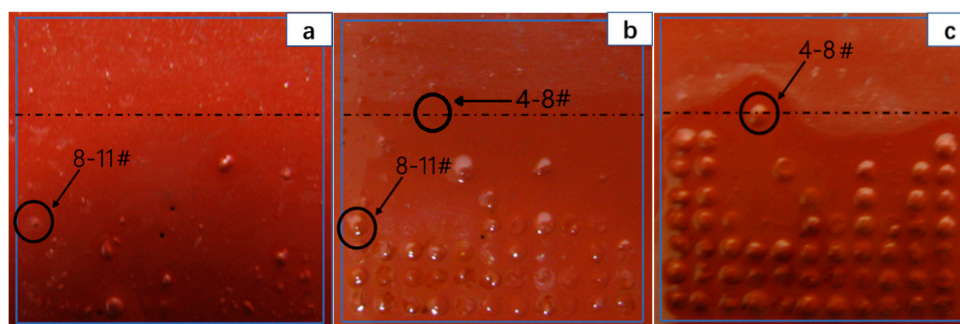


Figure 5. Cont.

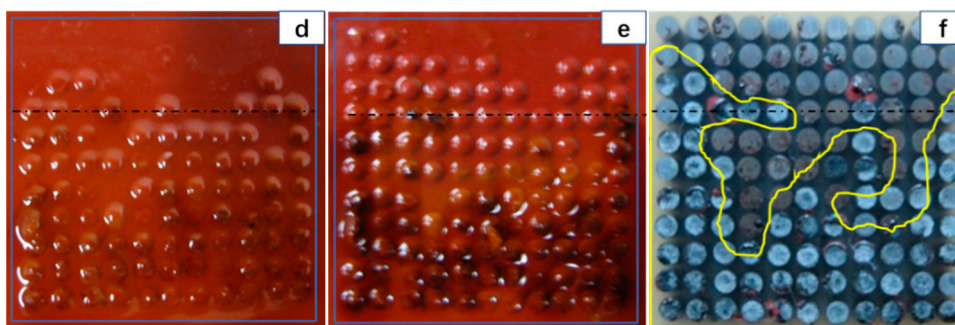


Figure 5. Morphology pictures of the coating surface immersed for (a) 12 days, (b) 21 days, (c) 29 days, (d) 47 days, (e) 76 days, and (f) the substrate under coating immersed for 76 days.

Oxygen reduction at the coating/metal interface is an important influencing factor that destroys the adhesion between the coating and the metal, leading to the delamination and delamination of coating [21,22]. For example, the 8–11# electrode behaved as the cathode for the first 30 days, and the cathode current density increased from 0.4 to $9.6 \mu\text{A}\cdot\text{cm}^{-2}$ across Day 12 to Day 21 (Figure 3c). On the 12th day, the surface coating of 8–11# showed slightly visible blisters and subsequently developed into obvious blisters on the 21st day, as shown in Figure 5a,b.

However, the interfacial cathodic reaction does not always lead to delamination. For example, the cathode current of the 4–8# electrode was significantly high on Day 21 (Figure 2c), but no delamination could be observed (Figure 5b). Until Day 29, the electrode (4–8#) showed a large anode current and blisters appeared (Figures 2d and 5c). Although the cathodic reaction can destroy the adhesion between the coating and the metal and cause the coating to peel off, delamination does not occur immediately due to the strong viscoelasticity of organic coating.

The cathode and anode current density distributions measured in the test are in good agreement with the corrosion morphology of the base metal. On the 76th day, the area of the anode current on the electrode surface (designated by the yellow curve) showed corrosion pits of different depths due to the dissolution reaction of the base metal. The surface of the substrate in the cathode reaction zone (outside the yellow curve) was free from corrosion, despite the loss of metallic luster (Figures 2f and 5f). The results also directly proved that WBE is a reliable testing technology for studying coating degradation and underlying metal corrosion processes.

3.4. Coating Deterioration and Underlying Metal Corrosion Processes in Water-Line Area

The degradation processes of the organic coating can be divided into three typical stages: water penetration, underlying corrosion initiation and corrosion development and expansion [9,23]. The coating degradation processes in the water-line area are mainly affected by water permeation and DACs. The first stage is the process of water penetration, as shown in Figure 6a. The ionic transport channels of the coating accelerate the water penetration process, and the corrosion of the base metal occurs preferentially [24]. The second stage is affected by water penetration and DACs, as shown in Figure 6b. The difference in aeration caused the cathodic reaction to occur adjacent to the water line while the anodic reaction occurred in the lower part [25]. The last stage is affected by water penetration, DACs, and thin liquid film, as shown in Figure 6c. When the cathodic zone extended to the gas phase area above the water line, this area becomes the strongest cathodic zone under the action of the thin liquid film. Affected by the non-uniform water penetration process of the coating and the DACs, the process of the coating degradation shows both randomness and regularity.

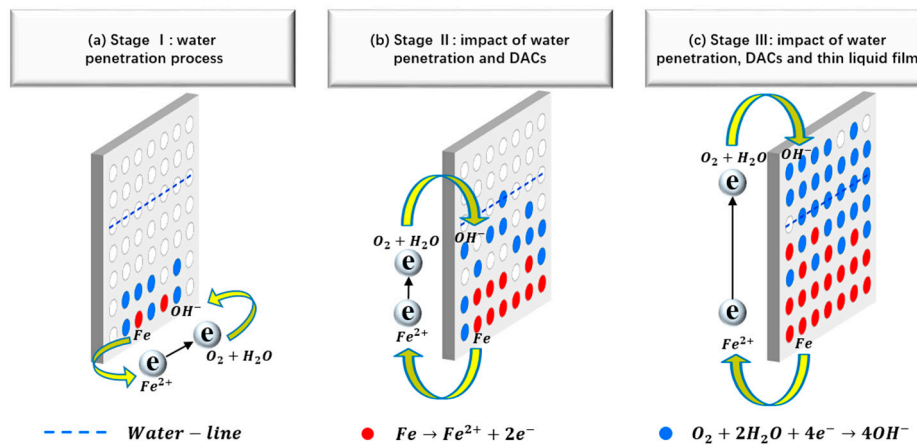


Figure 6. Schematic diagram of coating deterioration and underlying metal corrosion processes.

4. Conclusions

Coating deterioration and underlying metal corrosion processes in the water-line area were studied using the WBE technique in 3.5 wt.% NaCl solution. At the initial stage, the cathodic and anodic sites were randomly distributed across the coating due to the non-uniform water permeation processes. Affected by the DACs, the cathode reaction zone tended to be distributed above the anodic zone. As the polarity of the cathode points reversed to the anode, the coating was peeled and blistered from bottom to top. When the cathode region extended to the gas phase region above the water line, the region became the largest cathode current density region under the action of the thin liquid film. This significantly accelerated the corrosion of the base metal at the bottom. The increase in corrosion current was consistent with the increase in the delamination area on the coating surface. The WBE technique provides a new means of directly visualizing the role of DACs in coating deterioration and underlying metal corrosion processes in water-line area.

In the actual marine environment, coating degradation and metal corrosion in the water-line area are important corrosion phenomena with widespread influence, many influencing factors, and complex interactions. Coating degradation and metal corrosion in water-line area are not only affected by water permeation processes and DACs, but also affected by dynamic water level and micro/macro-organisms. In future experiments, we will explore the effects of dynamic water level and micro/macro-organisms separately. Finally, the influence of these factors on coating degradation and metal corrosion in the water-line area should be evaluated comprehensively.

Author Contributions: Conceptualization, W.Z. and W.L.; methodology, Z.C. and W.Z.; software, Z.C. and W.Z.; validation, Z.C. and Y.Z.; formal analysis, Z.C. and B.L.; investigation, Z.C. and B.L.; resources, W.Z. and W.L.; data curation, Z.C. and W.Z.; writing—original draft preparation, Z.C. and W.Z.; writing—review and editing, Y.Z. and T.S.; visualization, Z.C. and B.L.; supervision, W.Z. and W.L.; project administration, W.Z. and W.L.; funding acquisition, W.Z. and W.L. All authors have read and agreed to the published version of the manuscript.

Funding: This research was funded by the National Natural Science Foundation of China [grant numbers 51525903, 51879292, 21203034 and 51771057]; and GF research and cultivation project of Sun Yat-sen University [grant number 76110-18843406].

Conflicts of Interest: There are no conflicts of interest to declare.

References

1. Evans, U.R. *The Corrosion and Oxidation of Metals: Scientific Principles and Practical Applications*; Edward Arnold Pub. Ltd.: London, UK, 1960.
2. Tomashov, N.D. *The Theory of Corrosion and Protection of Metals*; MacMillan: New York, NY, USA, 1966.
3. Jeffrey, R.; Melchers, R.E. Corrosion of vertical mild steel strips in seawater. *Corros. Sci.* **2009**, *51*, 2291–2297. [[CrossRef](#)]

4. Tan, Y.J.; Bailey, S.; Kinsella, B. Mapping non-uniform corrosion using the wire beam electrode method. III. water-line corrosion. *Corros. Sci.* **2001**, *43*, 1931–1937. [[CrossRef](#)]
5. Tan, Y.J. Wire beam electrode: A new tool for studying localised corrosion and other heterogeneous electrochemical processes. *Corros. Sci.* **1998**, *41*, 229–247. [[CrossRef](#)]
6. Chen, Y.; Zhang, W.; Wang, W.; Wang, J.; Wang, Q.; Cai, G. Evaluation of water-line area corrosion for Q235 steel by WBE technique. *J. Chin. Soc. Corros. Prot.* **2014**, *34*, 451–458. [[CrossRef](#)]
7. Kong, D.; Wang, Y.; Zhang, W.; Wang, W.; Liu, X.; Wang, J. Correlation between electrochemical impedance and current distribution of carbon steel under organic coating. *Mater. Corros.* **2012**, *63*, 475–480. [[CrossRef](#)]
8. Wang, W.; Zhang, X.; Wang, J. The influence of local glucose oxidase activity on the potential/current distribution on stainless steel: A study by the wire beam electrode method. *Electrochim. Acta* **2009**, *54*, 5598–5604. [[CrossRef](#)]
9. Zhao, X.; Wang, J.; Wang, Y.; Kong, T.; Zhong, L.; Zhang, W. Analysis of deterioration process of organic protective coating using EIS assisted by SOM network. *Electrochem. Commun.* **2007**, *9*, 1394–1399. [[CrossRef](#)]
10. Cao, C. *Electrochemical Principle of Corrosion*; Chemical Industry Press: Beijing, China, 2004; ISBN 7502551875.
11. Ding, J.; Zhang, W.; Wang, J.; Chen, Y.; Yin, P.; Zhang, B. evaluation of water-line area corrosion for coating delamination by WBE technique-I. *J. Chin. Soc. Corros. Prot.* **2016**, *36*, 463–470. [[CrossRef](#)]
12. Morsch, S.; Lyon, S.; Gibbon, S.R. The degradation mechanism of an epoxy-phenolic can coating. *Prog. Org. Coat.* **2017**, *102*, 37–43. [[CrossRef](#)]
13. Leng, A.; Streckel, H.; Stratmann, M. The delamination of polymeric coatings from steel. Part 1: Calibration of the Kelvinprobe and basic delamination mechanism. *Corros. Sci.* **1999**, *41*, 547–578. [[CrossRef](#)]
14. Hamade, R.F.; Dillard, D.A. Assessing The effects of shear compression and peel on the cathodic degradation of elastomer-to-metal adhesive bonds. *Int. J. Adhes. Adhes.* **2005**, *25*, 147–163. [[CrossRef](#)]
15. Reddy, B.; Sykes, J.M. Degradation of organic coatings in a corrosive environment: A study by scanning kelvin probe and scanning acoustic microscope. *Prog. Org. Coat.* **2005**, *52*, 280–287. [[CrossRef](#)]
16. Jiang, J.; Wang, J.; Wang, W.; Zhang, W. Modeling influence of gas/liquid/solid three-phase boundary zone on cathodic process of soil corrosion. *Electrochim. Acta* **2009**, *54*, 3623–3629. [[CrossRef](#)]
17. Tsuru, T.; Nishikata, A.; Wang, J. Electrochemical studies on corrosion under a water film. *Mater. Sci. Eng.* **1995**, *198*, 161–168. [[CrossRef](#)]
18. Nishikata, A.; Ichihara, Y.; Hayashi, Y.; Tsuru, T. Influence of electrolyte layer thickness and pH on the initial stage of the atmospheric corrosion of iron. *J. Electrochem. Soc.* **1997**, *144*, 1244–1252. [[CrossRef](#)]
19. Liu, Z.; Wang, W.; Wang, J.; Peng, X.; Wang, Y.; Zhang, P.; Wang, H.; Gao, C. Study of corrosion behavior of carbon steel under seawater film using the wire beam electrode method. *Corros. Sci.* **2014**, *80*, 523–527. [[CrossRef](#)]
20. McCafferty, E. *Introduction to Corrosion Science*; Springer: New York, NY, USA, 2010; ISBN 9781441904546.
21. Furbeth, W.; Stratmann, M. The delamination of polymeric coatings from electro galvanised steel—A mechanistic approach. P 1: Delamination from a defect with intact zinc layer. *Corros. Sci.* **2001**, *43*, 207–227. [[CrossRef](#)]
22. Nazarov, A.P.; Thierry, D. Scanning Kelvin probe study of metal/polymer interfaces. *Electrochim. Acta* **2004**, *49*, 2955–2964. [[CrossRef](#)]
23. Zhang, W.; Wang, J.; Zhao, Z.; Liu, X. EIS Study on the deterioration process of organic coatings under immersion and cyclic wet-dry conditions. *J. Chin. Soc. Corros. Prot.* **2011**, *5*, 329–335. [[CrossRef](#)]
24. Zin, I.M.; Lyon, S.B.; Hussain, A. Under-film corrosion of epoxy-coated galvanised steel: An EIS and SVET study of the effect of inhibition at defects. *Prog. Org. Coat.* **2005**, *52*, 126–135. [[CrossRef](#)]
25. Wu, J.; Wang, P.; Gao, J.; Tan, F.; Zhang, D.; Cheng, Y.; Chen, S. Comparison of water-line corrosion processes in natural and artificial seawater: The role of microbes. *Electrochem. Commun.* **2017**, *80*, 9–15. [[CrossRef](#)]

